JOURNAL OF OPTOELECTRONICS AND ADVANCED MATERIALS Vol. 9, No. 1, January 2007, p. 114 - 120

Invited Lecture

Thermally-stimulated currents in thin-film semiconductors – computer modelling and experiment

C. MAIN*, Z. ANEVA[a], S. REYNOLDS, N. SOUFFI[b], D. NESHEVA[a] AND R. BRUGGEMANN[b]
University of Dundee, Division of Electronic Engineering and Physics, Dundee,DD1 4HN, UK.
[a]Institute of Solid State Physics, Bulgarian Academy of Sciences, 72 Tzarigradsko Chaussee Blvd., 1784 Sofia, Bulgaria
[b]Carl von Ossietzky Universitat, Fachbereich Physik, D26111, Oldenburg, Germany

We apply computer modelling to the multiple-trapping rate equations governing the time-evolution of non-equilibrium distributions of electrons and holes in extended and localised states in thin-film semiconductors, in thermally-stimulated conductivity measurements. We examine in detail the application of this method as a 'spectroscopy' of the energy distribution of localised states. Factors influencing energy and density scales are examined critically. Such factors include whether 'weak' or 'strong' re-trapping prevails during the measurement; the use of non-physical 'effective' attempt-to-escape frequencies; the effect of lifetime variation as distributions relax, and whether this can be measured accurately by supplemental steady-state photoconductivity. We show that in some circumstances, the energy scale can be approximated by the quasi-Fermi level position, and suggest further that the density of states may then be computed using the *derivative* of the quasi-Fermi energy with respect to temperature.

(Received November 28, 2006; accepted December 21, 2006)

Keywords: Thin films, Electrical properties, Computer simulation, Thermally stimulated currents

1. Introduction

Thermally stimulated conductivity (TSC) is a widely used and (superficially) simple experimental technique for investigation of the distribution of electronic states (DOS) in semiconductor materials. In practice, the method involves cooling a sample to low temperature, then illuminating for a set time to reach a steady state, in which gap states are occupied by excess charge carriers, and then after a short relaxation time in the dark, heating at a constant rate β Ks^{-1}.

Trapped charge is thermally excited from progressively deeper localised states as the temperature rises, and contributes to an excess free carrier density, e.g. for electrons n_{tsc}, and excess conductivity σ_{tsc}. As the temperature is raised, a narrow range of states around a gradually sinking energy $E_m(T)$ provides the greatest contribution to the thermal excitation rate at a given temperature T, and hence to σ_{tsc}. This 'peak emission' energy E_m sweeps downward toward the equilibrium Fermi energy E_{F0} until the material reaches thermal equilibrium. Measurement of σ_{tsc} during this process can give information on the DOS, $g(E)$.

Traditionally, the technique has been used for materials with localised states at well-defined energy levels. Here, the contribution of each level may ideally be described by a semi-analytic function, and the effect of several such states may, ideally, be considered as a superposition of each state's contribution. Analysis becomes a process of fitting a series of appropriately weighted functions to the total TSC curve, and numerous authors have published details of the relevant analyses [1-3].

In this paper, our starting point is that of an arbitrary continuous trap distribution, and rather than attempt to fit curves, we wish to attempt to demonstrate the use of the data 'spectroscopically' to find the DOS.

There are two limiting cases for the TSC relaxation process, commonly termed 'weak' and 'strong' re-trapping. In the former, the recombination time τ_R, for a free electron is shorter than the re-trapping time τ_{tm} in states 'around' E_m, so in a quasi-equilibrium approximation (small dn_{tsc}/dt), the instantaneous free electron density is determined only by the rates of emission at E_m and recombination. In the latter case, $\tau_{tm} < \tau_R$, and excess electrons are re-trapped a number of times 'near' E_m before recombining. Here, the descent of E_m may be substantially slowed, and now the instantaneous free electron density will be determined by the nett emission rate (emission minus re-trapping) at E_m, and recombination.

The criteria regarding the magnitudes of τ_{tm} and τ_R are significant; how do we define τ_{tm}? In a system with discrete trapping levels, we may clearly define τ_{tm} for each level. In a continuum of states, we need another definition. This is important, since it is not always clear whether weak or strong re-trapping prevails in a given measurement.

Furthermore, as the DOS is 'uncovered', the hole and electron quasi-Fermi levels approach one another, and the density of gap-centre states acting as recombination centres will decrease. Thus the carrier lifetimes will

change throughout the measurement and conditions may even change over from one regime (i.e. strong or weak re-trapping) to the other.

Interpretation of TSC requires establishment of energy and density scales from the data. Essentially, we link the energy scale to the temperature range and the density scale to the excess conductivity. In the case of weak re-trapping, with a constant lifetime, this is apparently straightforward. A number of authors [4-9] have analysed TSC in systems with continuous trap distributions and *weak* re-trapping, finding that irrespective of the detailed form of the DOS, a reasonably accurate energy scale *linearly* dependent on temperature (with a small offset) can be defined, typically of the form [6],

$$E_m(T) \approx kT \ln\left(\frac{41\nu_0}{\beta}\right) + 0.015\text{eV} \quad (1)$$

where ν_0 is the trap attempt-to-escape frequency for electrons, typically ~10^{12} s^{-1}, k is the Boltzmann constant and the factor 41 has dimensions of Kelvins. Without prior knowledge of ν_0 it may be thought reasonable to assume that we can determine its value from the temperature T_F at which E_m relaxes to the (known) equilibrium Fermi energy E_{F0}, when the TSC will decay very rapidly to zero, giving,

$$\nu_0 \approx \frac{\beta}{41}\exp\left(\frac{E_F - 0.015eV}{kT_F}\right). \quad (2)$$

It is further tempting to assume that this point occurs at the temperature at which σ_{tsc} has fallen to equal the dark conductivity σ_d. However, as we shall see below, neither definition may be valid in general, and the point may actually be inaccessible to measurement.

For strong re-trapping, the descent of E_m is slowed, by multiple trapping and release, but equations 1 or 2 have still been used to assign an energy scale, provided an *effective* attempt-to-escape frequency ν_{eff} is used, often *very much* smaller than ν_0 [9, 10]. This implicitly assumes that the descent of E_m is uniformly slowed throughout the measurement. It is not evident that this is a valid procedure, since the ratio τ_R/τ_{tm}, which determines the relative probabilities of retrapping and recombination, may vary throughout the measurement, and we address this also below.

The density scale for weak re-trapping may be obtained in the quasi-equilibrium case by considering the two rates; carrier release, as controlled by the descent rate of E_m through the distribution $g(E)$; and free carrier recombination. If states below E_m are fully occupied following initial optical excitation, then we may write,

$$\sigma_{TSC}(T) = e\mu\tau_R\beta\, g(E_m)\frac{dE_m}{dT} \quad (3a)$$

$$\approx \quad e\mu\tau_R\beta g(E_m)\left|\frac{E_m}{T}\right|, \quad (3b)$$

where Eq. 3b is obtained from Eq. 3a by using the linear relation of Eq. 1. Here, e is electronic charge, and μ is the free carrier mobility. This gives the result for the DOS,

$$g(E_m) \approx \frac{\sigma_{TSC}(T)}{e\mu\tau_R\beta\left|\frac{E_m}{T}\right|}. \quad (4)$$

It is not immediately clear whether Eq. 4 can be applied to the strong re-trapping case, since we must now equate only the *nett* de-trapping rate to the recombination rate. However, if the assumptions associated with adoption of ν_{eff} were valid, then Eq. 4, with an appropriately adjusted E_m, would be reasonable. We assess the validity of this notion in our numerical modelling, below.

A further complication, which applies to both weak and strong re-trapping, involves the *ad hoc* use of a variable temperature dependent lifetime $\tau_R(T)$ from experiment, in Eq. 3 [9, 11]. From the above, it is clear that this can vary during the experiment. Under the assumed quasi-equilibrium conditions, it is appropriate to use the prevailing value of $\tau_R(T)$.

The experimental problem is to measure the relevant value of τ_R, without significant perturbation of the TSC conditions. One suggested method [9] is to perform a separate determination of the $\mu\tau_R$ product by steady-state photoconductivity (SSPC), whilst ensuring that the photoconductivity (and hence the excess electron density) is equal to σ_{tsc} (n_{tsc}) at the same temperature. In this way, it is assumed that the trapped electron and hole densities are also identical to those in the TSC experiment, giving the same lifetime. While this seems reasonable, we note that the prevailing conditions in the two experiments are different; in SSPC there is an additional optical generation rate. We also address this last point in our numerical modelling, below.

2. Numerical simulation

We represent the continuous DOS $g(E)$ by a ladder of discrete levels of density $N_{ti} = g(E_i)\Delta E$ (cm^{-3}), where ΔE is the energy spacing. Both electron and hole trapping kinetics are included, to give the following coupled differential equations for the densities of free electrons, holes and trapped electrons; n, p and n_{ti} respectively.

$$\frac{dn}{dt} = -n\sum_i c_{ni}(N_{ti} - n_{ti}) + \sum_i e_{ni}n_{ti} + G_{opt} \quad (5a)$$

$$\frac{dp}{dt} = -p\sum_i c_{pi}n_{ti} + \sum_i e_{pi}(N_{ti} - n_{ti}) + G_{opt} \quad (5b)$$

$$\frac{dn_{ti}}{dt} = nc_{ni}(N_{ti} - n_{ti}) - e_{ni}n_{ti} + pc_{pi}n_{ti} - e_{pi}(N_{ti} - n_{ti}) \quad (5c)$$

In Eqs. 5a,b,c, c_{ni}, c_{pi}, e_{ni}, e_{pi} represent the coefficients for electron and hole capture, and the emission rates, respectively. Hopping conduction, studied in [12], is not considered here.

The loosely coupled differential equation set Eq. 5a,b,c may be solved for the various conditions encountered in TSC and SSPC measurements, for time-dependent solutions in all variables, and also steady state values, by an implicit stiff solver routine developed first for the isothermal transient photocurrent decay, outlined in earlier publications [13, 14], replacing when required, the fixed T by a linear ramp $T = T_0 + \beta t$.

Simulation proceeds much as experiment. Thermal equilibrium conditions simply require setting the optical generation rate G_{opt} to zero, and time stepping out to sufficiently long times. Illumination at low temperature, relaxation and temperature ramping are simulated, and the variation of the excess electron density $n_{\rm tsc}$ with T is obtained by subtracting the computed value of the thermal electron density $n_{\rm d}$ from the total density. The only addition made, to find $\tau_R(T)$, is a second simulated TSC temperature scan, with supplemental optical generation at a level so low (typically 1.0 $cm^{-3}s^{-1}$) that it produces insignificant perturbation of the TSC curve. This allows the carrier lifetimes to be calculated accurately, in a way not possible by experiment.

3. Results and discussion

3.1. Simulations

The first TSC simulation reported is for a simplified system which has a constant density of states of 10^{16} $cm^{-3}eV^{-1}$, extending from E_C to 0.8 eV below E_C. E_F is placed at a 0.7 eV depth, $c_n = 10^{-8}$ cm^3s^{-1} and $\nu_0 = 10^{12}$ s^{-1}. The base temperature is 90K and β = 0.05 Ks^{-1}. We further restrict the treatment in this case to electrons only, and localised states above E_{F0}, and include a recombination term $-n/\tau_R$ *explicitly* in Eq. 5a. Fig. 1 shows the temperature dependence of the excess and dark electron density for different values of the lifetime τ_R from 10^{-4} s to 10^{-10} s. Since the trapping time into states within $2kT$ of E_m lies between $1 - 3\times10^{-6}$ s, regions of weak and strong re-trapping can be identified.

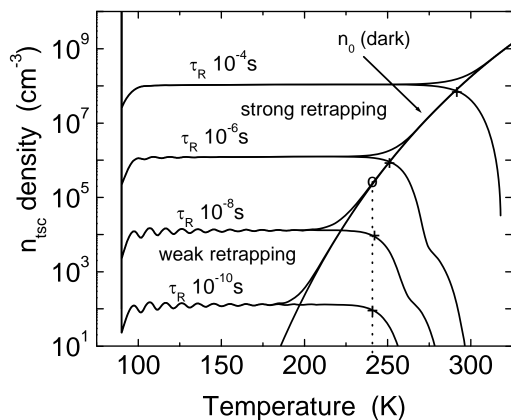

Fig. 1. TSC curves. Parameter - τ_R 10^{-10} to 10^{-4} s for 'flat' DOS $g(E) = 10^{16}$ $cm^{-3}eV^{-1}$.

Using Eq.1, we can find the temperature at which E_m should reach E_{F0}. A value of 237K is obtained, and this is indicated by a dashed line in Fig. 1. It is clear that this is valid for the weak re-trapping regime, and occurs when $n_{\rm tsc} \ll n_{\rm dark}$, while for strong re-trapping, the 'turn-down' when $E_m = E_F$, occurs at higher temperatures, and when $n_{\rm tsc} = n_{\rm dark}$.

The point at which $n_{\rm tsc} = n_{\rm dark}$ moves continuously to higher temperatures as the lifetime τ_R is increased through both régimes, so it is difficult to associate this with a single energy scale.

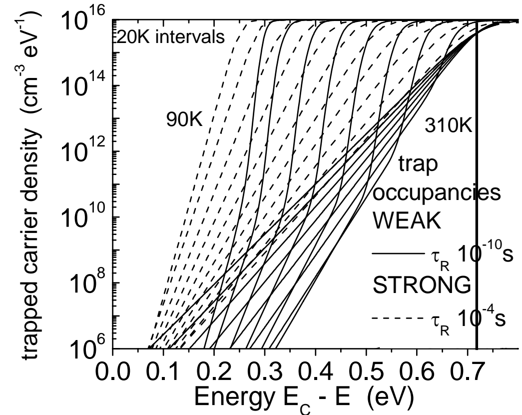

Fig. 2. Energy distributions of trapped electrons at 20 K intervals for the weak and strong re-trapping cases, in a 'flat' DOS.

Fig. 2 illustrates, for representative weak and strong re-trapping cases, contrasting the energy distributions of trapped electrons. For strong re-trapping, the distribution is Boltzmann-like over the range $E_C - E_m$, while for weak re-trapping, E_m descends more quickly, and there is a sharp fall near E_m followed by a Boltzmann-like distribution

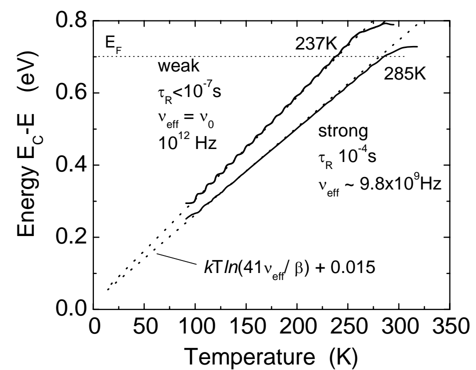

Fig. 3. Variation of peak emission energy Em, with temperature in weak and strong re-trapping régimes. for a flat DOS.

for shallow states. This neatly demonstrates why the excess free carrier density in the weak re-trapping case can be much less than the equilibrium density when the relaxation is complete, i.e. at the turnover point. Also, the figure implies that the quasi-Fermi energy must be close to the emission peak energy, for strong re-trapping.

Fig. 3 plots the progress of E_m with temperature for representative weak and strong re-trapping cases, compared with Eq. 1. It can be seen that Eq. 1 does predict the temperature T_F at which E_m reaches E_F, for weak re-trapping, with the appropriate ν_0. For strong re-trapping, there is again a linear, but slower, descent of E_m with T, consistent throughout with a lower ν_{eff}. Whether such a simple 'all-temperature' re-scaling applies in more general cases is studied below.

Our more recent simulations include a more realistic DOS, and both electron and hole transitions. Fig. 4 illustrates a model DOS used in these simulations

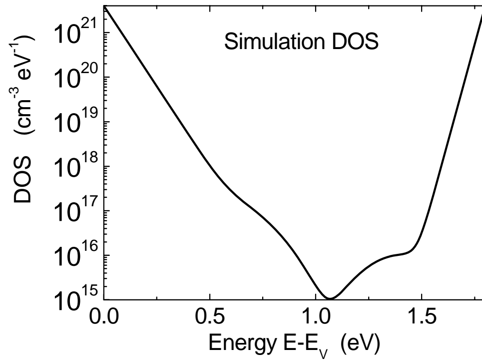

Fig. 4. Model density of states used in simulations. E_V is the top of the valence band.

In this model, the conduction band and valence band tails have characteristic energies of 25 and 60 meV respectively. Two Gaussian distributions of defect states are included, centred at energies 0.4 and 1.2 eV below the conduction band edge E_c, with peak densities 10^{16} and 10^{17} $cm^{-3}eV^{-1}$ respectively and widths (standard deviation) 0.14 eV. Setting all capture coefficients to 10^{-8} cm^3s^{-1} results in weak re-trapping conditions, while strong re-trapping conditions for electrons can be reproduced, mainly by appropriate adjustment of hole capture coefficients to $10^{-10}cm^3s^{-1}$, within reasonable physical limits.

Fig. 5 shows simulated TSC curves for the excess electron density for the model DOS, for cases of weak and strong re-trapping. Regions of high TSC are seen at low and high temperatures. In this more complete model, the carrier lifetime will vary automatically with temperature, and this variation is shown in Fig. 6. As the temperature rises, and the quasi-Fermi levels relax inward, the electron lifetime in each case increases. The appearance of a peak and a more level variation at higher temperatures simply indicates that the lifetime at these temperatures (above the TSC measurement range) is controlled by the thermal occupation of deep states.

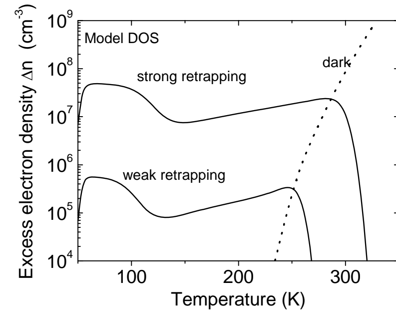

Fig. 5. Simulated TSC curves of excess electron density for model DOS of Fig. 4. The weak and strong re-trapping cases are shown.

As a check on whether weak or strong re-trapping conditions prevail in these simulations, it is possible to compute the ratio of the trapping rate/recombination rates for the group of traps around E_m each contributing more than, say, 25%
of the peak nett emission produced by the trap at E_m. By nett emission, we mean the difference between the emission and trapping rates for the given trap.

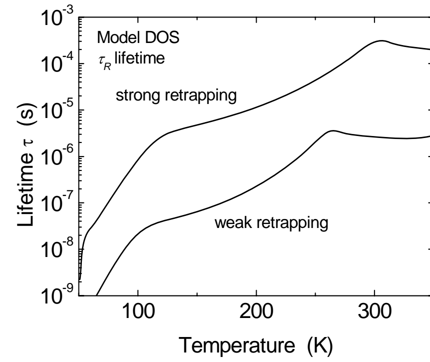

Fig. 6. Computed electron lifetime from simulated TSC for the model DOS. The weak and strong re- trapping cases are shown.

If the ratio defined above is greater or less than unity, then this indicates strong or weak re-trapping, respectively. This function is shown in Fig. 7, for the two simulated cases. It can be seen that the chosen parameters do produce the required conditions.

In Fig. 8, we show, for the model DOS, the variation of the computed energy of peak emission *vs* temperature for the *weak* re-trapping case. Also in the figure are the approximate linear result of Eq.1, for the appropriate ν_o of 10^{12} Hz, and the quasi-Fermi energy E_{Fn} computed from the free electron density, using either of the following:

$$E_{Fn} = E_{F0} + kT \ln\left(\frac{I_{TSC}}{I_{dark}}\right) \quad (6a)$$

$$E_{Fn} = kT \ln\left(\frac{N_C e\mu EA}{I_{TSC} + I_{dark}}\right). \quad (6b)$$

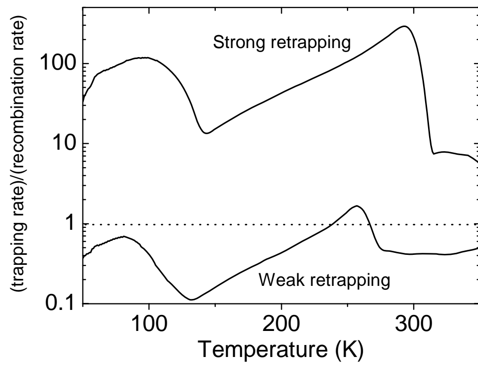

Fig. 7. Computed ratio of the trapping rate/recombination rate in the model DOS, for those traps whose nett emission is more than 25% of the peak emitting trap. A ratio of unity defines the weak - strong criterion.

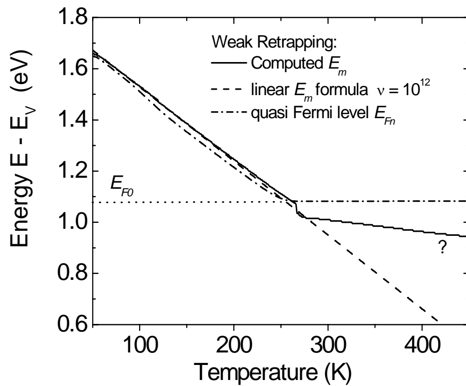

Fig. 8. Weak re-trapping case. Computed peak emission energy vs temperature for the model DOS. Also shown: the linear approximate result of Eq.1 and the quasi-Fermi energy E_{Fn}.

It can be seen that in this case, the linear result of Eq.1 is a good estimate of E_m over most of the temperature range, while E_{Fn} is also close to E_m.

It is noticeable that the simulation shows E_m continuing to fall at high temperatures, *below* the dark Fermi energy E_{F0}. At these temperatures, the excess TSC charge has almost vanished, and we are close to thermal equilibrium. Although a value for E_m can still be computed in this temperature range, indicating a peak in emission from the lower set of defect states, the nett emission rate is now very small as detailed balance is approached.

Using the data of Figs. 5, 6 and 7, the DOS can be calculated according to Eq. 4 to assess the accuracy of the 'reconstruction' technique. However, Fig. 8 indicates that there are two possible ways to create the required energy scale. We may simply apply the linear relation of Eq. 1, with some initial estimate for ν_0, or we may use the value for E_{Fn}, found from the data, using Eq. 6a or 6b. The result of this calculation is shown in Fig. 9. Both energy scales are reasonably good in reproducing the DOS.

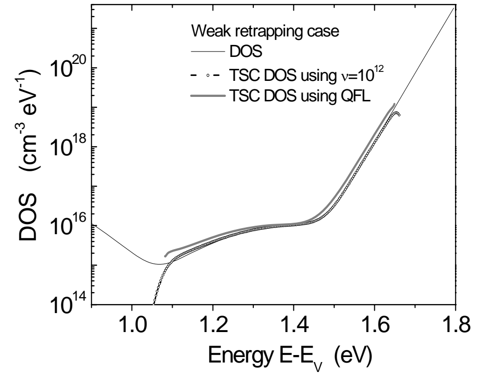

Fig. 9. DOS computed by Eq. 4 from simulated TSC for the model system under weak re-trapping conditions, comparing Eq. 1 and Eq. 6 for the energy scaling.

Fig. 10 shows the comparison, for the weak re-trapping case, of the computed trapped carrier distributions in TSC and SSPC measurements at 200K, arranged so that the free electron density is the same for each measurement. There is only a small difference evident, but note that a log scale is in use. It appears that there are slightly sharper 'edges' to the distributions in the TSC case, as might be expected from Fig. 2. The carrier lifetimes are not identical as was assumed for the purposes of employing this technique. The TSC computed lifetime is 2.3×10^{-7} s, while the SSPC lifetime is 2.9×10^{-7} s, some 26% greater, and this discrepancy will affect the accuracy of the DOS determination.

Turning to the strong re-trapping case, Fig. 11 shows, for the model DOS, the variation of the computed energy of peak emission E_m *vs* temperature. Also in the figure is the approximate linear result of Eq. 1, for the appropriate ν_o of 10^{12} Hz, an effective ν_{eff} of 10^{10} Hz and the quasi-Fermi energy E_{Fn} computed from the free electron density. It can be seen that now the variation of E_m is curved and that neither linear approximation seems to be a good fit, and that E_{Fn} follows E_m rather well.

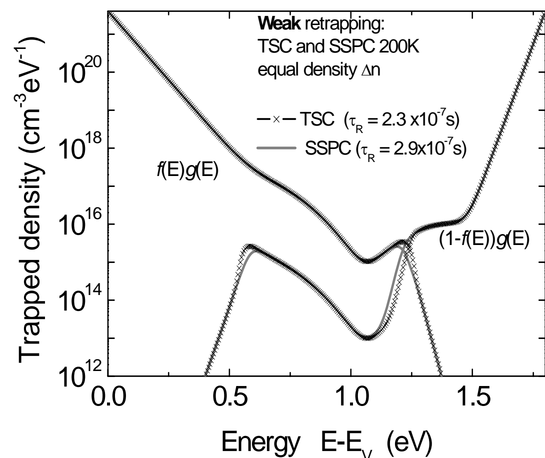

Fig. 10. Comparison of the trapped carrier distributions at 200K for TSC and SSPC, arranged to give identical free electron densities (weak re-trapping).

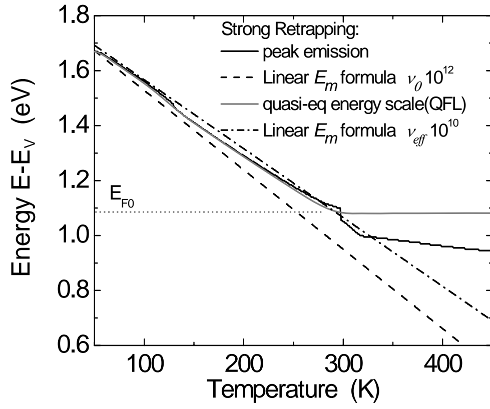

Fig. 11. Strong re-trapping case. Computed peak emission energy vs temperature for the model DOS. Also shown: a linear approximate result of Eq. 1 for $v_0 = 10^{12}$ Hz, $v_{eff} = 10^{10}$ Hz, and the quasi-Fermi energy E_{Fn}.

This last observation suggests a different approach to the calculation of the DOS. Since the relation here between E_m and T is non-linear, and since E_{Fn} follows E_m well, (as expected for strong re-trapping), then use of Eq. 4 may be less appropriate for the DOS. Instead, replacing dE_m/dT with dE_{Fn}/dT in Eq. 3a gives a novel variant of Eq. 4, *viz-*

$$g(E_m) \approx \frac{\sigma_{TSC}(T)}{e\mu\tau_R\beta\left|\frac{dE_{Fn}}{dT}\right|} \tag{7}$$

Thus, Eq. 6 and Eq. 7 can be used to compute the energy and density scales for the DOS, without the need to use possibly inappropriate linear approximations or dubious concepts like v_{eff}.

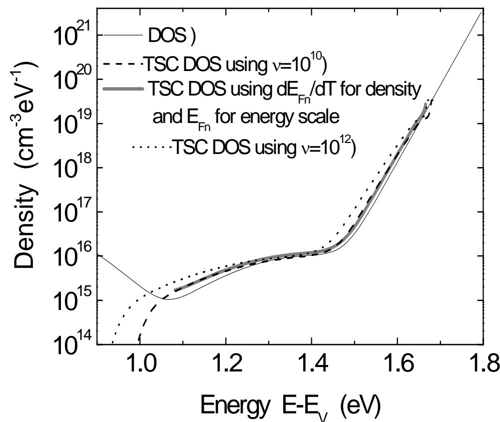

Fig.12. DOS computed from simulated TSC for the model system under strong re-trapping conditions, using Eq.1 and 4 for $v_0=10^{12}$ and $v_{eff}=10^{10}$ Hz, and also using E_{Fn} via Eq.6 and 7 .

Fig. 12 shows the original DOS and computed DOS, using several options. The first two involve using the linearly-varying E_m of Eq. 1 with $v_0 = 10^{12}$ and $v_{eff} = 10^{10}$ Hz respectively. The third plot uses E_{Fn} and its derivative dE_{Fn}/dT to compute the energy and density scales. It can be seen that forstrong re-trapping, the use of the actual v_0 gives an incorrect result, while the use of v_{eff} or the use of E_{Fn} both, in this case, give better fits.

Computed trapped carrier distributions at 200K for SSPC and TSC are again very similar as was the case with weak re-trapping, while the SSPC lifetime is some 18% greater than the TSC computed lifetime.

3.2. Experiment

Fig. 13 shows experimental TSC results for a HWCVD microcrystalline Si:H sample. The preparation data were: 300°C deposition, 5% SiH_4/H_2, thickness 2μm, crystalline volume fraction ~ 79%. The mobility-lifetime product *vs* temperature is shown in Fig. 14, where the measurement was made at $I_{SSPC} = I_{TSC}$ as described

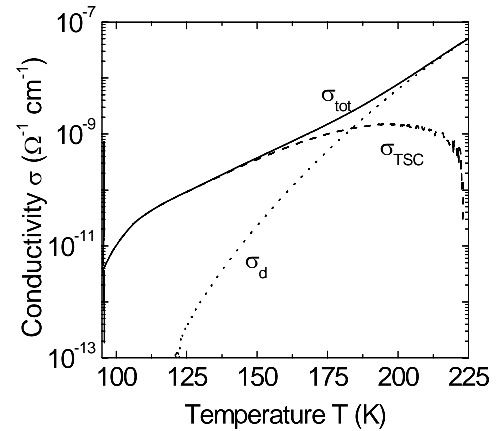

Fig. 13. Experimental TSC on a microcrystalline Si:H sample.

above. Over much of the temperature range, at least up to the point where $I_{TSC} = I_{dark}$, it appears that the variation of E_{Fn} with T is close to linear, so in this case, the linear approximation technique is valid, and unfortunately the data cannot be used as a demonstration of the suggested technique. Work

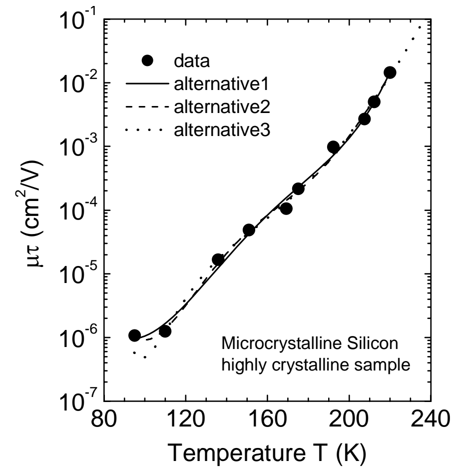

Fig. 14. Measured mobility-lifetime product for thesample in Fig. 13, using the $I_{SSPC} = I_{TSC}$ criterion. Several alternative fits to the data are shown.

is proceeding on this topic. It seems that strong re-trapping is in force throughout this measurement, and from the point at which $I_{TSC} = I_{dark}$, a value of $\nu_{eff} = 1.4\times10^7$ was estimated. Figure 15 shows the computed DOS for the material.

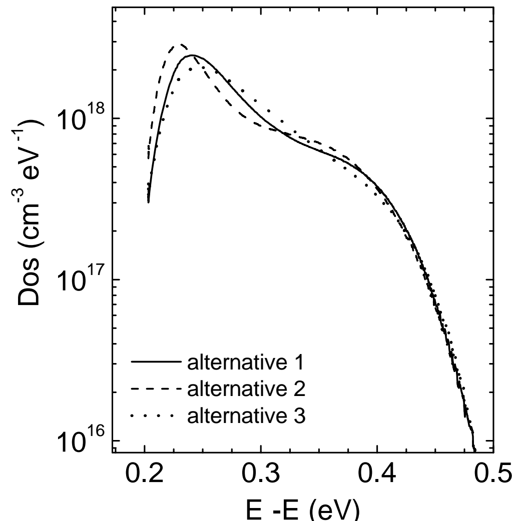

Fig.15. Density of states determined from TSC and mobility-lifetime data.

4. Conclusions

It has been demonstrated that TSC measurements may be used in a 'spectroscopic' manner to determine the DOS for relatively slowly varying trap distributions, without making the assumptions underlying the standard 'curve-fitting' often used for discrete traps. The validity of the previously suggested technique for finding the appropriate mobility-lifetime product has been tested, and we find that relatively small errors arise from this technique. In the case of strong re-trapping, we suggest an alternative to the use of 'effective' attempt-to-escape frequencies in the establishment of an energy scale, proposing that the quasi-Fermi level is a good alternative. Furthermore, we suggest that the derivative dE_{Fn}/dT may be used in determining the density scale, so that measured values (i.e the TSC) are used to more effect in the determination of the DOS, rather than semi-analytic approximations.

Acknowledgements

This study was supported by NATO Collaborative Linkage Grant PST.CLG.980656, and a British Council, DAAD-ARC joint research project grant 1185. We also wish to thank J. Guillet and J.bE. Bourée, Ecole Polytechnique, Palaiseau, France for provision of microcrystalline silicon samples.

References

[1] T. A. T. Cowell, J. Woods, Brit. J. Appl. Phys. **18**, 1045 (1967).
[2] S. G. Elkomoss, M. Samimi, M. Hage-Ali, P. Siffert, J. Appl. Phys. **57**, 531 (1985).
[3] Z. Aneva, D. Nesheva, E. Vateva, J. Appl. Phys. **100**, 053704 (2006).
[4] G. Landweer, J. Bezemer, in Amorphous silicon and related materials, Ed. H. Fritzsche World Scientific Singapore (1988), p 525.
[5] J. G. Simmons, G. W. Taylor, M. C. Tam, Phys. Rev. B **7**, 3714 (1973).
[6] J. G. Simmons, M. C. Tam, Phys. Rev. B **7**, 3706 (1973).
[7] D. S. Misra, A. Kumar, S. C. Agarwal, Phys. Rev. B **31,** 1047 (1985).
[8] J. A. Schmidt, R. R. Koropecki, R. Arce, A. Dussan, R. H. Buitrago, J Non-Cryst. Solids **338-340**, 322, (2004).
[9] M. Zhu, H. Fritzsche, Philos. Mag. B **53**, 41 (1986).
[10] M. Zhu, Appl. Phys. A **52**, 285, (1991).
[11] J. A. Schmidt, R. R. Koropecki, R. Arce, A. Dussan, R. H. Buitrago, J Non-Cryst. Solids **338-340**, 322 (2004).
[12] S. D. Baranovskii, M. Zhu, T. Faber, F. Hensel, P. Thomas, M. B. von der Linden, W. F. van der Weg, Phys. Rev. B **55**, 16226, (1997).
[13] C. Main, D. Nesheva, J Optoelectron. Adv. Mater. **3**, 655 (2001).
[14] C. Main, J. Non-Cryst. Solids **299-302**, 525 (2001).

*Corresponding author: c.main@dundee.ac.uk